Available online at www.sciencedirect.com

ScienceDirect

Journal of the European Ceramic Society 30 (2010) 2337–2344

www.elsevier.com/locate/jeurceramsoc

Physical characterization and arcjet oxidation of hafnium-based ultra high temperature ceramics fabricated by hot pressing and field-assisted sintering

Matthew Gasch *, Sylvia Johnson

NASA Ames Research Center, MS 234-1, Moffett Field, CA 94035, United States

Available online 1 May 2010

Abstract

For this study, HfB_2-based ultra high temperature ceramic (UHTC) samples were prepared by hot pressing and field-assisted sintering (FAS) with 10–20 vol.% SiC (baseline), 5 vol.% $TaSi_2$, and 5 vol.% iridium. Dense billets were tested for hardness and mechanical strength. When compared, the FAS method consistently yielded materials with a grain size 1.5–2 times finer than samples processed via hot pressing. In general, room temperature flexural strengths of these materials were found to be lower (∼400 MPa) than similar fully dense HfB_2–SiC materials, with strengths between 500 and 700 MPa. Oxidation resistance testing of flat-face models was conducted in a simulated re-entry environment, at $Q_{\text{Cold Wall}}$ ∼250 W/cm^2 for 5 min. Samples processed by FAS had reduced oxide thickness and SiC depletion zones compared to the baseline HfB_2–20SiC material. In all cases oxide thickness was reduced by ∼3× and SiC depletion zone thickness was reduced ∼3× over the baseline.
Published by Elsevier Ltd.

Keywords: Hot pressing; Sintering; Hafnium diboride; Oxidation resistance; Composites

1. Introduction

Ceramic borides, such as hafnium diboride (HfB_2) and zirconium diboride (ZrB_2), are members of a family of materials with extremely high melting temperatures referred to as ultra high temperature ceramics (UHTCs). UHTCs constitute a class of promising materials for use in high temperature applications, such as sharp leading edges on future-generation re-entry vehicles, because of their high melting points.[1]

Despite their potential, wide scale use has been limited, due, in part, to poor fracture toughness and oxidation resistance. Several researchers have looked at modifying the material composition to improve the performance of these materials.[2–5,26,27]. However, careful consideration must be given to the grain boundary phases, formed during processing with additives, as these can deteriorate the strength, thermal performance, and physical properties of UHTCs at elevated temperatures.[6,7]

The controlled development of microstructure has become important to the processing of UHTCs, with the prospect of improving the mechanical and thermal properties of these materials.[8–12] The improved oxidation resistance of HfB_2 has also become important if this material is to be successfully used at temperatures above 2000 °C. The current study has investigated processing HfB_2-based materials with SiC, $TaSi_2$, and iridium powder.

The addition of $TaSi_2$ was pursued in this work based on the previous work of several researchers. Talmy et al. investigated the oxidation of ZrB_2 ceramics with SiC, Si_3N_4, Ta_5Si_3 and $TaSi_2$ additions and found that all additions improved the oxidation resistance of ZrB_2/SiC ceramics below 1400 °C.[19] They found that improved oxidation resistance correlated with modification of the chemical composition of the surface oxide layer, leading to decreased inward diffusion of oxygen. Furthermore Peng and Speyer demonstrated that $TaSi_2$ additions improved the oxidation of ZrB_2 materials up to 1550 °C.[18]

Iridium is also well known for its high temperature oxidation resistance, moreover the addition of metallic or semi-metallic sintering aids such as Fe, Ni, Co, W, WC have been shown to improve final density of Hf and Zr-based ceramics and these additions allow for lower densification temperatures.[21]

In addition to the investigation of additives for improving oxidation resistance and processing temperature of Hf-based composites, two processing techniques were evaluated in this work; conventional hot pressing as well as electric field-assisted

* Corresponding author at: NASA Ames Research Center, Thermal Protection Materials Branch, MS 234-1, Bldg 234, Room 211, Moffett Field, CA 94035, United States. Tel.: +1 650 604 5377; fax: +1 650 604 0487.

E-mail address: matthew.j.gasch@nasa.gov (M. Gasch).

0955-2219/$ – see front matter. Published by Elsevier Ltd.
doi:10.1016/j.jeurceramsoc.2010.04.019

sintering (FAS). The resulting microstructural variations were evaluated with SEM; the mechanical strength of each sample was evaluated using bi-axial flexure; and oxidation behavior of these materials was evaluated in a simulated re-entry environment in the AHF arcjet facility at NASA Ames Research Center, during a 5-min exposure to a cold wall heat flux of ∼250 W/cm^2 and stagnation pressure of 0.1 atm.

2. Experimental procedure

The raw powders used in this work were: −325 mesh HfB_2 and $TaSi_2$ from Cerac Inc., 1–2 μm SiC from H.C. Starck Inc., and −325 mesh iridium from SurePure. Analysis of the crystalline phases present in the raw and mixed powders was performed with X-ray diffraction (Scintag X-ray diffractometer) using Cu kα radiation. Particle size of the raw and milled powders was measured using laser light scattering (Malvern). Powders were then weighed according to volume % of each material and then wet-milled them with WC(Co) milling media in a planetary mill (Fritsch Pulverisette 5, Germany). The milled powders were carefully dried to prevent phase segregation between the HfB_2 (ρ = 11.12 g/cm^3) and the SiC (ρ = 3.2 g/cm^3). After drying, the powders were loaded into a 25 mm diameter graphite die lined with graphfoil. Hot pressing was conducted in a graphite element resistance furnace (Thermal Technologies HP50-7010G, Santa Rosa, CA) with vacuum levels of <200 mTorr. Above 1600 °C, the partial pressure of carbon in the furnace increased significantly and degraded the vacuum. Consequently, we back-filled the furnace with one atmosphere of inert gas (argon or helium), to preserve the graphite element and insulation. Typical furnace conditions required for densification were 1900–2200 °C for 1 h at 25 MPa.

Field-assisted sintering (FAS) was conducted at the AFOSR labs in Dayton, OH. The FAS system there is a FCT System GmbH Model HPD 25-1 (Rauenstein, Germany). We used the same milled powders as those densified by conventional HP. Samples were again loaded into a 25 mm diameter graphite die lined with graphfoil. Typical conditions required for FAS densification were 1800–1900 °C, with hold times of 5–10 min. Ramp rates used during FAS ranged from 100 to 300 °C per minute. Sample temperature was measured by an optical pyrometer focused on the bottom of a bore hole in the punch ∼5 mm from the powder.

Density of the hot-pressed billets and test specimens was measured using the Archimedes method. After the samples were cross-sectioned and polished to a 1-μm finish, we characterized the microstructure of consolidated samples using optical microscopy, scanning electron microscopy (FEI ESEM 30, Hillsborough, OR) with EDX analysis and transmission electron microscopy (FEI TEM CM200FEG, Philips, Eindhoven, Netherlands) operating at 200 kV. Average grain size was determined using the lineal intercept method without grain shape corrections, following ASTM E112.

TEM (FEI TEM CM200FEG, Philips, Eindhoven, Netherlands) specimens were prepared using a method developed for thinning ceramic fibers, but the technique is equally applicable to bulk samples.[22,23] Samples were sectioned with a low-speed diamond saw into thin slices and then mechanically ground and polished to 5–10 μm thickness with the aid of a tripod polisher using successively finer diamond lapping films. Final thinning was accomplished by mounting the thin sections on 50-mesh copper grids followed by low-angle ion milling (Precision Ion Polishing System, Gatan, Pleasanton, CA) to electron transparency. Energy-dispersive X-ray spectroscopy (Model Voyager, Noran Instruments, Middleton, WI) was used for elemental analysis.

Mechanical and thermal property test specimens were prepared with diamond tooling and ground to a final surface finish in accordance with ASTM C1161 (Chand Kare Technical Associates, Worcester, MA). Vickers hardness was determined using indentations created with a Shimadzu indenter (HSV-30, Japan). Hardness values were calculated from the average length of the diagonal lines across an indentation made by applying a load of 49 N over a 15-s interval. Flexural strength was measured using bi-axial flexure testing, according to ASTM 1499 "Monotonic Equibiaxial Flexure Testing," using 25.4 mm diameter × 2 mm thick disks with a crosshead speed of 0.5 mm/min.

The laser flash diffusivity technique was used (Netzsch LFA457, Germany), over the range 25–600 °C to measure thermal diffusivities. Samples were coated with a light spray of carbon powder to prevent reflection of the incident laser beam. Measurements were made under vacuum, using a laser (1538 V setting) with a pulse duration of 0.5 ms. Signals were corrected to account for heat losses using Cowen + Pulse correction method.[25] We repeated thermal diffusivity measurements three times at each temperature, and averaged the results, arriving at extremely repeatable measurements, with typical standard deviations of less than 0.5%. Conversion to thermal conductivity requires numerical values for the density and specific heat at the corresponding temperatures. We used the measured room temperature densities of each sample, considering the effect of thermal expansion range insignificant over the temperature range measured. The method used to calculate specific heat values for all samples is reported elsewhere.[24]

Finally, oxidation resistance was conducted on machined flat-face models in a simulated re-entry environment created via the NASA Ames Advanced Heating Facility (AHF) arcjet. A photo of an as-machined flat-face arcjet model is shown in Fig. 1. The model is 25.4 mm in diameter, and the overall height is 8 mm. The notch in the base of the model, shown in the lower left of Fig. 1, is used to pin the model into the holder. Models were placed in SiC-coated graphite holders (shown in the right-most image of the same figure), enabling test durations in excess of 10 min. Models and holders were then attached to a water-cooled arm (sting) that moved the models in and out of the plasma stream.

A variety of instrumentation was used to calibrate arcjet conditions and measure the thermal response of the materials. Cold wall heat flux values, shown in Table 1, were measured using a copper Gardon gauge and are referenced to a 76 mm diameter hemisphere. However, hot wall heat flux values at the model's surface differ, because of differences in model geometry and between the catalycity of the models and the catalycity of the copper Gardon gauge (detailed discussion of the heat flux at the

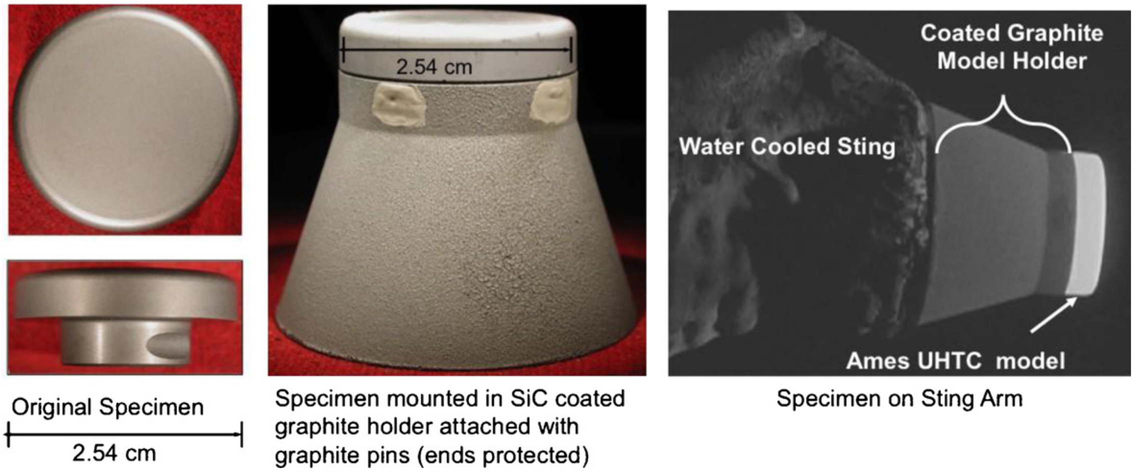

Fig. 1. Flat-face arcjet model shown as fabricated, attached to SiC-coated graphite holder and attached to water-cooled sting arm.

surface of the model is beyond the scope of this work). Two-color optical pyrometers were used to make surface temperature measurements during the tests.

Oxide thickness of post-arcjet models was determined after models were cross-sectioned and polished to a 1-μm finish and then inspected under SEM as described above. Oxide thickness was determined by averaging 5–8 thickness measurements across an image that was taken at the middle of the model (12 mm from either edge).

3. Results and discussion

3.1. Processing and properties

Table 1 shows the average particle size, crystalline phases present, and surface area of the as-received powders. After milling, the average particle size of the powder mixtures is ~2.1 μm. Table 2 lists the physical characteristics of the consolidated samples. The densities of consolidated samples ranged from 94 to 99% of the theoretical density (TD). Fig. 2 shows SEM micrographs of polished cross-sections. The dark phase in the images is SiC and the lighter phase is HfB_2. $TaSi_2$ additions are hard to distinguish from the HfB_2 phase, because of the similar atomic weight; however, for the sample with iridium, the iridium phase is the brightest color and is clearly distributed at grain boundaries and triple points in the hot-pressed sample. The FAS sample with iridium had much less time for solid-state diffusion, and the iridium grains appear more equiaxed, like that of the hafnium phase. Upon analysis of the billet post-processing, cracks were visible in the FAS sample with iridium, within the bulk material; thus, we did not measure some properties, such as hardness and strength, on this material.

Table 2 summarizes the experimental values of some mechanical properties. Vickers hardness values for the materials processed during this work are between 13 and 18 GPa. The hot-pressed samples with $TaSi_2$ and iridium have hardness values on the low end, in part due to the slight porosity of those samples. However, the FAS sample with $TaSi_2$ had the highest hardness, possibly a result of a reduced grain size, despite also having the lowest theoretical density.

Average strengths of the baseline HfB_2–SiC material ranged from 428 to 485 MPa, for the FAS and hot-pressed samples, respectively. Average strengths for the samples with $TaSi_2$ ranged from 330 to 380 MPa; again the hot-pressed material had the highest strength. It is interesting to note that the addition of $TaSi_2$ to the baseline material resulted in lower average strengths. The addition of 5 vol.% iridium and $TaSi_2$ to the baseline resulted in hot-pressed samples with a reduced grain size. However, the same materials processed via FAS cracked; thus, hardness and strength were not measured. In general, the room temperature flexural strengths of these materials is rather low compared to results reported on similar fully dense HfB_2–SiC materials.[9,17] In fact, samples processed by FAS consistently had lower strength values, despite having refined grain size. These results are somewhat contrary to the expected result; higher strengths were expected for the samples processed by FAS. Research by Guo et al.[12] on ZrB_2-based composites found that the flexural strength of samples fabricated with nano-sized SiC particles was much higher than samples processed with micron-sized SiC. The observed increase in strength was attributed to SiC particles within ZrB_2 grains forming in situ inter-granular

Table 1
Summary of the properties of the starting powders used in this study.

Vendor	Powder	Surface area (m^2/g)	Particle size (d0.5) (μm)	Crystalline phases detected
Starck	HfB_2	0.43	4.1	HfB_2/HfC
Starck	SiC	8.09	1.6	SiC
Cerac	$TaSi_2$	–	4.6	$TaSi_2$
SurePure	Ir	0.15	11.6	Ir

Table 2
Summary of the physical characterizations done on consolidated samples processed in this study.

Sample ID	Hot-pressed properties			
	Density (g/cm^3)	Grain size (μm)	Hardness (HV)	Strength (MPa)
HfB_2–20SiC (Baseline)	9.49 (99% TD)	7.7	16.5	485
HfB_2–10SiC–5$TaSi_2$	9.45 (96% TD)	8.5	13.0	380
HfB_2–15SiC–5$TaSi_2$–5Ir	9.98 (96% TD)	5.1	13.0	–
Sample ID	**Field assist sintered properties**			
	Density (g/cm^3)	Grain size (μm)	Hardness (HV)	Strength (MPa)
HfB_2–20SiC (Baseline)	9.46 (99% TD)	4.1	17.5	428
HfB_2–10SiC–5$TaSi_2$	9.61 (94% TD)	2.3	18.0	330
HfB_2–15SiC–5$TaSi_2$–5Ir	10.02 (97% TD)	1.6	–	–

SiC, $TaSi_2$ and Ir amounts represent volume % of each addition.

composites. Thus, while the fabrication of UHTC composites by FAS creates refined grains, an improvement in flexural strength is likely not possible without the fabrication of materials using nano-sized starting powders.

Thermal conductivity measurements were performed on all materials, as a function of temperature from 25 to 600 °C; see Fig. 3. There is a significant difference between the pure HfB_2, fabricated in a previous study from elemental powders via FAS,[27] and the baseline HfB_2–SiC materials fabricated at ARC. Materials originally hot pressed at ARC under a previous program used a long process that resulted in material that has a room temperature conductivity of ~40 W/mK. In this study, the processing of the baseline material via FAS results in an ~2× increase in conductivity, to ~80 W/mK at room temperature. Preliminary research indicates that the migration of impurities from grain boundaries into the bulk HfB_2 during long hot-pressing times are the main reason for reduced thermal conductivity.[24] As shown in Fig. 4, TEM analysis demonstrates that Mg, Al and oxygen contaminates could be found in several locations. Cobalt contamination (from the WC(Co) milling media) was also detected at grain boundaries, however, tungsten and tantalum were not found in grain boundaries. Increased processing times could allow the electronic structure/vacancy concentration of bulk HfB2 and SiC to be altered either via the diffusion of impurities from grain boundaries into the bulk or by the loss of boron or carbon during processing.[24,27] The baseline HfB_2–SiC materials presented in this paper were processed with a modified hot-press schedule that, while shorter than the

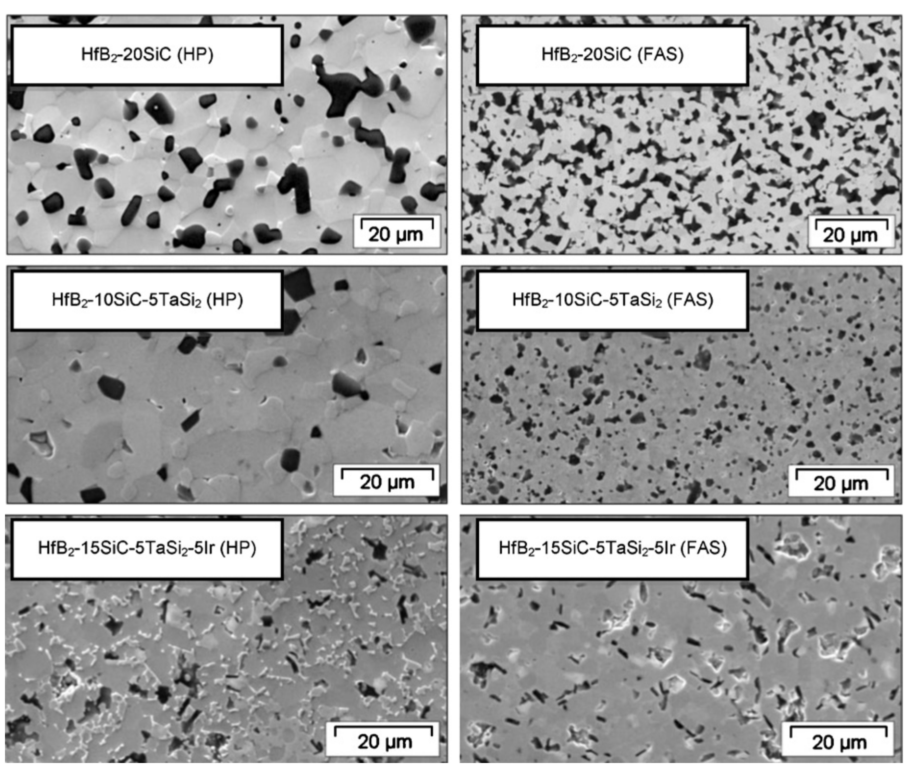

Fig. 2. SEM images of the current UHTC samples comparing the differences in microstructure between hot pressing and field-assisted sintering.

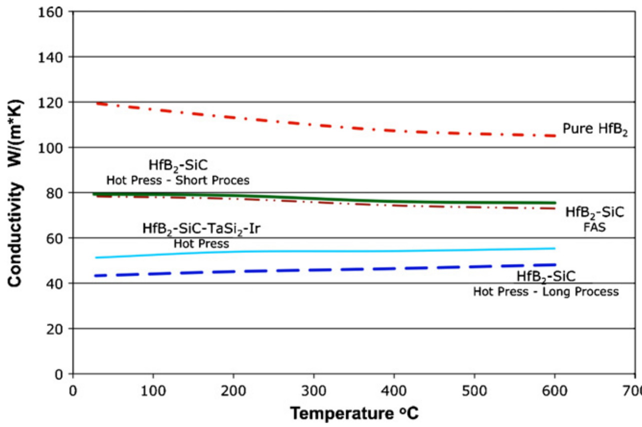

Fig. 3. Thermal conductivity as a function of temperature for each of the materials presented in this paper.

previous schedule, is 6× longer than samples processed by FAS. Interestingly, baseline (HfB_2–20SiC) materials hot pressed with the shorter schedule demonstrate thermal conductivity similar to materials processed by FAS. However, the addition of $TaSi_2$ and/or iridium to the baseline powder yields material with a conductivity reduced to ~50 W/mK at room temperature.

3.2. Arcjet testing

Fig. 5 provides a comparison of the surfaces of each of the flat-face models after arcjet exposure at ~250–280 W/cm^2 for 5 min. A comparison of the measured surface temperatures and post-test emittance is listed in Table 3. For the baseline HfB_2/SiC samples, steady state surface temperatures were ~1690 °C for the hot-pressed material and ~1530 °C for the FAS processed sample. The higher temperature observed on the hot-pressed sample can be attributed to the formation of a more uniform oxide scale, whereas the FAS sample appears to have oxidized less across the surface. Post-test emittance measurements confirm that the FAS sample has a thinner oxide layer, as this sample had a much higher emittance. A similar trend was observed for the samples with $TaSi_2$ additions, where the surface temperature for the hot-pressed sample was ~45 °C higher than the FAS sample. The sample with $TaSi_2$ and Ir additions exhibited surface temperatures ~100 °C lower than the baseline hot-pressed material and ~30 °C higher than the sample with $TaSi_2$ additions and no Ir additions. Interestingly, the surfaces of samples with SiC and $TaSi_2$ additives remained smooth during testing and after cooldown. However, droplets were observed to have formed on the sample with Ir during testing. In the post-test surface image, droplets of iridium (confirmed by EDX analysis) dot the otherwise smooth surface of the model.

In previous studies by ManLabs and others, the oxidation of HfB_2/SiC samples was observed to leave three distinct regions within the material.[1,13–16] The first region comprises the surface oxide, primarily composed of SiO_2 and some HfO_2. Below that is a SiC-depleted zone, where the SiC has oxidized away (active oxidation), leaving behind a porous HfB_2 matrix. Below the depletion zone is virgin material.

The flat-face models tested in this series were cross-sectioned to determine if a similar structure had formed. Fig. 6 shows the SEM images of the cross-sections of each arcjet sample. Each sample clearly shows a white SiO_2 oxide layer, below which is a SiC-depleted region of porous HfB_2 grains. A comparison of the measured oxide thickness and SiC depletion zone thickness for each sample is listed in Table 3. In general, the oxidation resistance of samples with $TaSi_2$ additions is better than the baseline HfB_2–SiC materials, as expected.[18,19] A comparison of hot-pressed materials shows the addition of $TaSi_2$ reduced

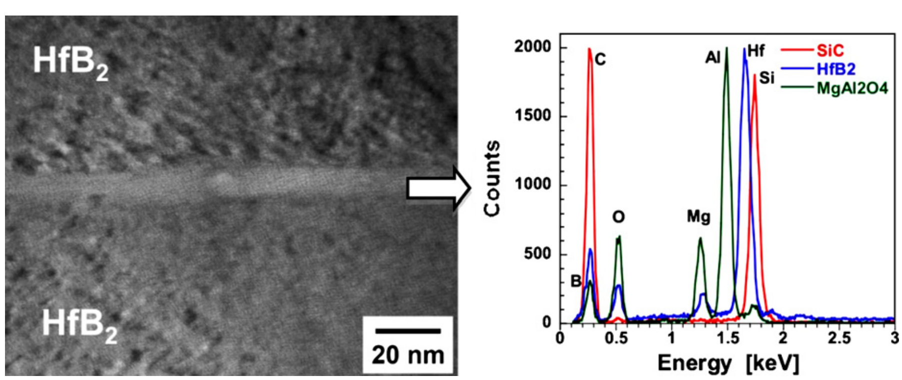

Fig. 4. TEM images of the current and spectra of some impurities at the grain boundaries of hot-pressed HfB_2–20SiC material processed using a long hold time.

Table 3
Summary of the arcjet conditions, surface temperature, post-test emittance and oxide thickness of cross-sectioned arcjet models.

Sample ID	Sintering method	CW heat flux (W/cm^2)	P_{stag} (atm)	Test duration (s)	Surf. temp. (°C)	Post-test emittance	Oxide thickness (μm)	SiC depletion (μm)
HfB_2–20SiC (Baseline)	Hot press	280	0.19	600	1690	0.67	13	24
HfB_2–20SiC (Baseline)	FAS	250	0.10	600	1530	0.87	3	8
HfB_2–10SiC–5$TaSi_2$	Hot press	250	0.10	600	1560	0.89	7	34
HfB_2–10SiC–5$TaSi_2$	FAS	250	0.10	600	1515	0.89	3	6
HfB_2–15SiC–5$TaSi_2$–5Ir	Hot press	250	0.10	600	1590	0.87	4	9

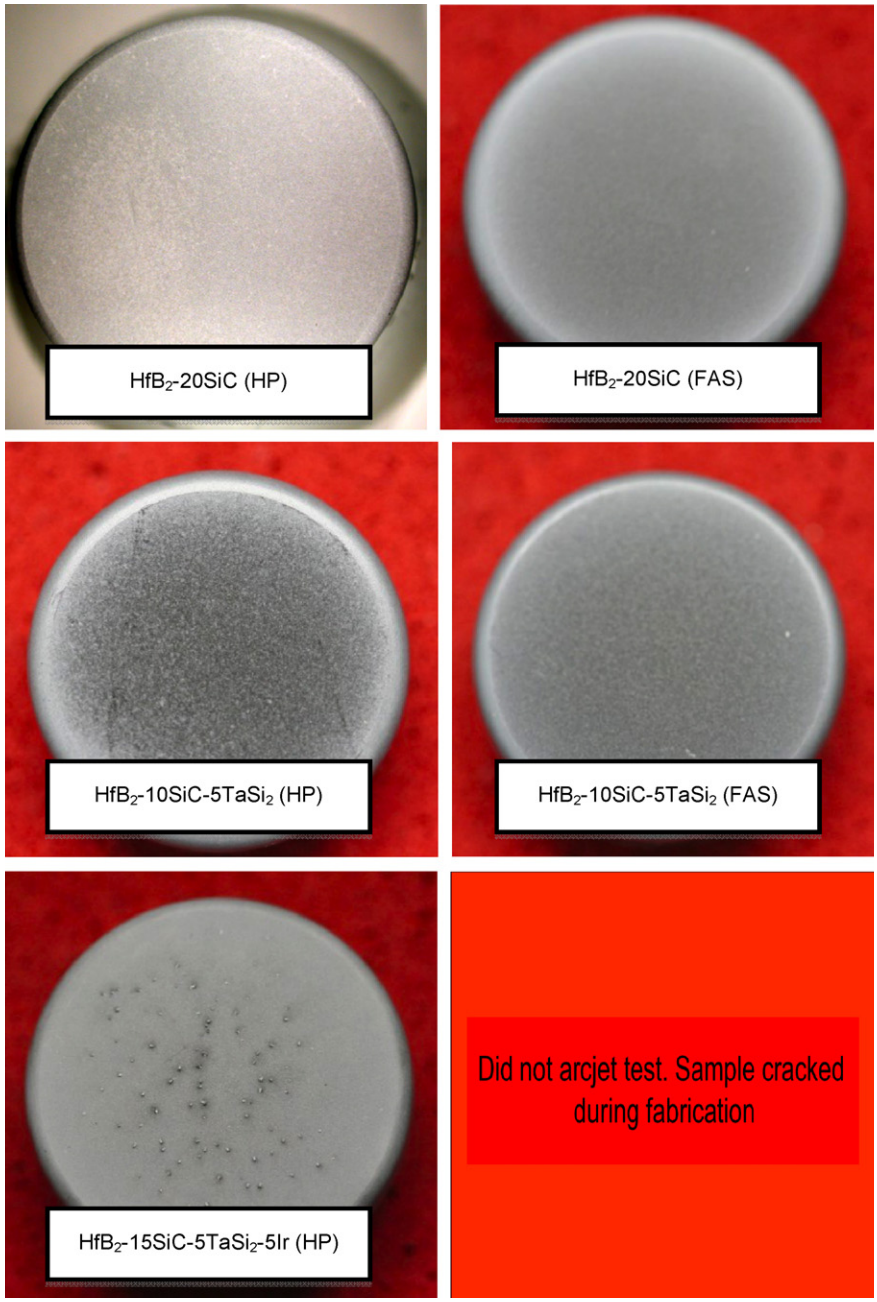

Fig. 5. Images of the surface of each of flat-face models after 5-min arcjet exposure.

oxide thickness by 2× but, the SiC depletion zone was ∼1.5× larger than the baseline material. Interestingly, the addition of $TaSi_2$ and Ir reduced oxide thickness by 3×. The iridium appears insoluble in HfB_2 and can be observed along grain boundaries and triple points, perhaps acting as an oxygen barrier around HfB_2 grains.

All samples processed by FAS had reduced oxide thickness and SiC depletion zones. In all cases, oxide thickness was reduced by ∼3× and SiC depletion zone thickness was reduced ∼3× over the baseline. Very recently, Hwang et al.[20] reported that the incorporation of nano-sized SiC particles improved the oxidation resistance of hot-pressed ZrB_2 ceramics. The results of our work appear to support their hypothesis, that ceramics with reduced grain size have an increased diboride/SiC interface length per unit area of exposed surface and a decreased spacing between Si-containing particles. The decrease in spacing between SiC particles allows the surface to more rapidly form a protective oxide over the diboride phase.

More arcjet testing is required to improve our understanding of the oxidation mechanisms within these materials in high temperature oxidizing environments. Additional testing is also required to verify the reproducibility of the current results. However, these results, though preliminary, suggest that further improvements in the oxidation resistance of HfB_2 materials can be realized by achieving small-grained microstructures with well distributed SiC or $TaSi_2$ dispersions. Finally, the addition

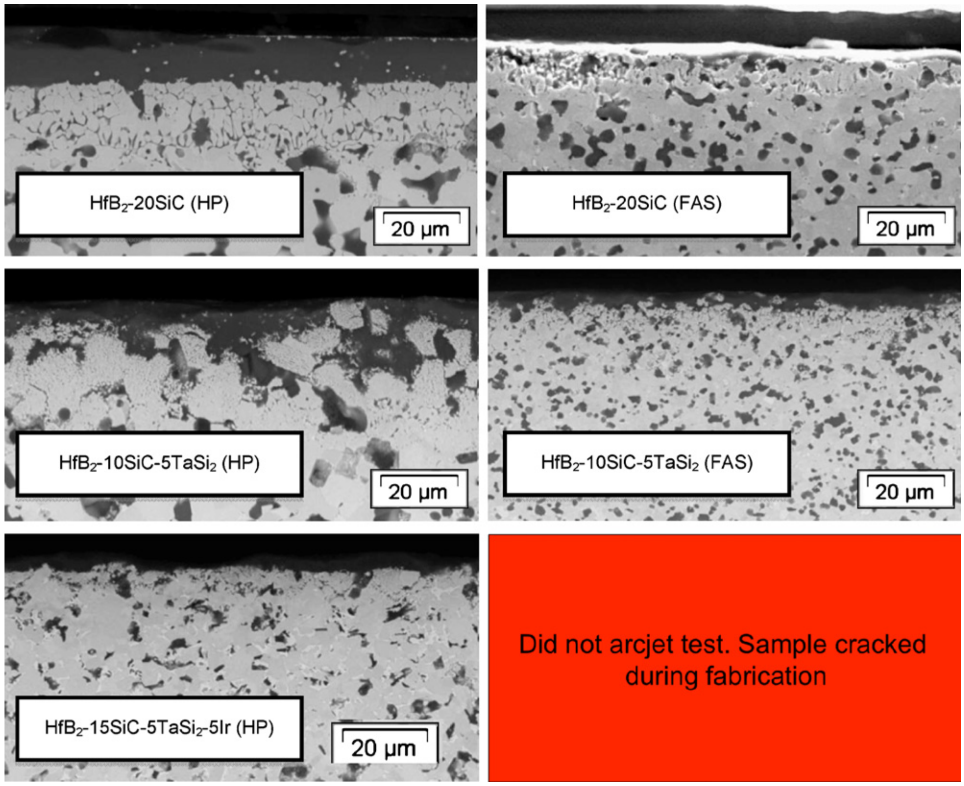

Fig. 6. Cross-sectional images of each of the arcjet models post-test.

of iridium also appears to reduce oxidation of these materials perhaps by acting as an oxygen barrier around HfB_2 grains.

4. Conclusions

Three different ultra high temperature ceramics: HfB_2 + 20 vol.% SiC (baseline), HfB_2 + 10 vol.%SiC + 5 vol.%$TaSi_2$, and HfB_2 + 5 vol.% $TaSi_2$ + 5 vol.% iridium, were prepared by hot pressing and field-assisted sintering (FAS). In comparison to hot pressing, the FAS method consistently yielded materials with a grain size 1.5–2× finer than samples processed via hot pressing. Consolidated specimens were tested for hardness and mechanical strength via bi-axial flexure of 25 mm diameter × 2 mm thick disks. Samples processed by FAS consistently had lower strength values, despite having refined grain size, and, in general, the room temperature flexural strengths of these materials were found to be low (~400 MPa) compared to results reported on similar fully dense HfB_2–SiC materials that showed strengths between 500 and 700 MPa.

Oxidation resistance was characterized in a simulated re-entry environment in the Ames AHF arcjet facility. Testing of flat-face models was conducted at $Q_{\text{Cold Wall}}$ ~250 W/cm^2 for 5 min. All samples processed by FAS had reduced oxide thickness and thinner SiC depletion zones than the baseline HfB_2–20SiC material that was hot pressed. In all cases, oxide thickness was reduced by ~3× (from ~13 to ~3 μm) and SiC depletion zone thickness was reduced ~3× (from ~24 to ~8 μm) over the baseline. The results of the work presented here appear to support the work of others, whereby diboride ceramics fabricated with reduced SiC grains have an increased diboride/SiC interface length per unit area of exposed surface and a decreased spacing between Si-containing particles. The decrease in spacing between SiC particles allows the surface to more rapidly form a protective oxide over the diboride phase.[20]

Acknowledgments

This work was funded by the Hypersonics element of the Fundamental Aeronautics Program at NASA Aeronautics Research Mission Directorate (ARMD). Michael Cinibulk of the Materials and Manufacturing Directorate, Air Force Research Laboratory, performed the TEM work. We also acknowledge NASA-SCAP for their critical financial support of the arc-jet operational capability at Ames. Portions of this work were also performed under NASA contract NAS2-99092 to ELORET Corp. We would like to thank Jerry Ridge of ELORET for his support measuring the surface emittance of UHTC arcjet samples.

References

1. Kaufman L, Clougherty EV. *Investigation of boride compounds for high temperature applications, RTD-TRD-N69-73497. Part XXXVII*. Cambridge, MA: ManLabs Inc.; 1963.
2. Guo S-Q. Densification of ZrB_2-based composites and their mechanical and physical properties: a review. *J Eur Ceram Soc* 2009;**29**:995–1001.
3. Guo W-M, Vleugels J, Zhang G-J, Wang P-L, Van der Biest O. Effects of Re2O3 (Re = La, Nd, Y and Yb) additions in hot-pressed ZrB2–SiC ceramics. *J Eur Ceram Soc* 2009;**29**:3063–8.

4. Li G, Han W, Zhang X, Han J, Meng S. Ablation resistance of ZrB_2–Sic–AlN ceramic composites. *J Alloys Compd* 2009;**479**:299–302.
5. Sciti D, Silvestroni L, Nygren M. Spark plasma sintering of Zr- and Hf-borides with decreasing amounts of $MoSi_2$ as sintering aid. *J Eur Ceram Soc* 2008;**28**:1287–96.
6. Monteverde F, Bellosi A. *J Mater Res* 2004;**19**:3576.
7. Monteverde F, Guicciardi S, Bellosi A. *Mater Sci Eng A* 2003;**34**:6310.
8. Ni D-W, Zhang G-J, Kan Y-M, Sakka Y. Textured HfB_2-based ultra high temperature ceramics with anisotropic oxidation behavior. *Scripta Mater* 2009;**60**:913–6.
9. Monteverde F. Progress in the fabrication of ultra high temperature ceramics: 'in-situ' synthesis, microstructure, and properties of a reactive hot-pressed HfB_2–SiC composite. *Compos Sci Technol* 2005;**65**:1869–79.
10. Chen L, Gu Y, Shi L, Yang Z, Ma J, Qian J. Synthesis and oxidation of nanocrystalline HfB_2. *J Alloys Compd* 2004;**36**:8353–6.
11. Zhang X, Xu L, Du S, Han W, Han J. Crack-healing behavior of zirconium diboride composite reinforced with silicon carbide whiskers. *Scripta Mater* 2008;**59**:1222–5.
12. Guo S-Q, Yang J-M, Tanaka D, Kagawa Y. Effect of thermal exposure on strength of ZrB_2-based composites with nano-sized SiC particles. *Compos Sci Technol* 2008;**68**:3033–40.
13. Gasch M, Ellerby D, Irby E, Beckman S, Gusman M, Johnson S. Processing, properties and arcjet oxidation of hafnium diboride-silicon carbide ultra high temperature ceramics. *J Mater Sci* 2004;**39**:5925–37.
14. Monteverde F. The thermal stability in air of hot-pressed diboride matrix composites for uses at ultra-high temperatures. *Corros Sci* 2005;**47**:2020–33.
15. Savinao R, De Stefano Fumo M, Silverstrioni L, Sciti D. Arc-jet testing on HfB2 and HfC-based ultra-high temperature ceramic materials. *J Eur Ceram Soc* 2008;**28**:1899–907.
16. Zhang X, Hu P, Han J, Meng S. Ablation behavior of ZrB_2–SiC ultra high temperature ceramics under simulated atmospheric Re-entry conditions. *Compos Sci Technol* 2008;**68**:1718–26.
17. Monteverde F, Melandri C, Guicciardi S. Microstructure and mechanical properties of HfB_2 + 30 vol.% SiC composite consolidated by spark plasma sintering. *Mater Chem Phys* 2006;**100**:513–9.
18. Peng F, Speyer RF. Oxidation resistance of fully dense ZrB_2 with SiC, TaB_2 and $TaSi_2$ additives. *J Am Ceram Soc* 2008;**91**(5):1489–94.
19. Talmy IG, Zaykoski JA, Opeka M. High-temperature chemistry and oxidation of ZrB_2 ceramics containing SiC, Si_3N_4, Ta_5Si_3 and $TaSi_2$. *J Am Ceram Soc* 2008;**91**(7):2250–7.
20. Hwang SS, Vasiliev AL, Padture NP. Improved processing and oxidation-resistance of ZrB_2 ultra-high temperature ceramics containing SiC nanodispersoids. *Mater Sci Eng A* 2007;**464**:216–24.
21. Monteverde F, Bellosi A, Guicciardi S. Processing and properties of zirconium diboride-based composites. *J Eur Ceram Soc* 2002;**22**:279–88.
22. Cinibulk MK, Welch JR, Hay RS. Preparation of thin sections of coated fibers for characterization by transmission electron microscopy. *J Am Ceram Soc* 1996;**79**(9):2481–4.
23. Cinibulk MK, Welch JR, Hay RS. Transmission electron microscopy specimen preparation of ceramic coatings on ceramic fibers. *Mater Res Soc Symp Proc* 1997;**480**:3–17.
24. Gasch M, Johnson S, Marschall J. Thermal conductivity characterization of hafnium diboride-based ultra high temperature ceramics. *J Am Ceram Soc* 2008;**91**(5):1423–32.
25. Cowan RD. Pulse method of measuring thermal diffusivity at high temperatures. *J Appl Phys* 1963;**34**(4):926–7.
26. Opila E, Levine S, Lorincz J. Oxidation of ZrB_2- and HfB_2-based ultra high temperature ceramics: effect of Ta additions. *J Mater Sci* 2004;**39**(19):5969–77.
27. Zhang SC, Hilmas GE, Fahrenholtz WG. Improved oxidation resistance of zirconium diboride by tungsten carbide additions. *J Am Ceram Soc* 2008;**91**(1):3530–5.